PERGAMON

International Journal of Heat and Mass Transfer 46 (2003) 1097–1102

International Journal of HEAT and MASS TRANSFER

www.elsevier.com/locate/ijhmt

The effect of large-amplitude g-jitter vertical free convection boundary-layer flow in porous media

D. Andrew S. Rees [a,*], Ioan Pop [b]

[a] Department of Mechanical Engineering, University of Bath, Bath BA2 7AY, UK
[b] Department of Mathematics, University of Cluj, Cluj CP253, Romania

Received 8 August 2002

Abstract

In this paper we consider how the boundary-layer flow induced by a constant temperature vertical surface embedded in a porous medium is modified by time periodic variations in the gravitational acceleration. It is assumed that the amplitude of these variations is comparable with the mean gravitational acceleration. The resulting nonsimilar boundary layer equations are solved using the Keller-box method after using a Fourier decomposition in time to reduce the system to parabolic form with only two independent variables. The main effect of such g-jitter is confined mainly to the region near the leading edge and becomes weak at larger distances from the leading edge. For small g-jitter amplitudes the numerical results compare very well indeed with our earlier analysis in Rees and Pop [Int. Comm. Heat Mass Transfer 27 (2000) 415].
© 2002 Elsevier Science Ltd. All rights reserved.

1. Introduction

Due to its numerous applications in a wide variety of industrial processes as well as in many natural circumstances, the subject of convective flow in porous media has attracted considerable attention in the last few decades. Examples of such technological applications are geothermal extraction, storage of nuclear waste material, ground water flows, thermal insulation engineering, food processing, fibrous insulation, soil pollution and packed-bed reactors to name just a few. For a list of the key references of a vast literature concerning this subject, we refer to the most recent books by Nield and Bejan [2], Ingham and Pop [3] and Vafai [4].

Convective flows in both viscous (nonporous) and in fluid-saturated porous media are driven by buoyancy forces resulting from the presence of both a temperature gradient and a gravitational field. However, there has been great deal of recent interest in the effects of those buoyancy forces which are produced by the interaction of density gradients with the variable acceleration field known as g-jitter. There is a growing literature which tries to characterize the g-jitter environment and the review articles by Alexander [5] and Nelson [6] give a good summary of earlier work on convective flows in viscous fluids. There have also been a number of recent studies which investigate the effect of g-jitter on such fluids, e.g. [7–14]; these papers also provide references to earlier work on the subject. However, to the best of our knowledge there is very little work in the published literature which is devoted to the study of g-jitter effects on convective flows in porous media (see [1]).

All the above-mentioned studies show that convection in a microgravity environment is related to the magnitude of g-jitter and to the alignment of the growth direction (in crystal growth) or the direction of the temperature gradient (in convective flows). Several calculations, which are based on numerical models, have been made to estimate and calculate the adverse effects of time-varying g-jitter (see [13]). Both 2-D and 3-D numerical models have been developed for this purpose. These models have been used to study the effects associated with both idealised single-and multiple-frequency g-jitter modulation and realistic g-jitter data collected by

* Corresponding author. Tel.: +44-225-826775; fax: +44-225-826928.
E-mail address: d.a.s.rees@bath.ac.uk (D.A.S. Rees).

0017-9310/03/$ - see front matter © 2002 Elsevier Science Ltd. All rights reserved.
PII: S0017-9310(02)00369-1

accelerometer during real flight experiments. Studies have shown that the frequency, amplitude and spatial orientation of the residual gravity vector all play an important role in determining the convective flow behaviour of the system. When the residual accelerations oscillate in a particular direction, the orientation of this direction relative to the density gradient determines whether a mean flow is generated in the system. Sinusoidal oscillating accelerations induce an oscillating convective flow and composition oscillation in the liquid pool during crystal growth. The resulting velocity and composition fields usually oscillate with the same frequency as the imposed gravity field.

The aim of the present paper is to study the behaviour of the g-jitter induced free convection in the boundary-layer over a vertical flat plate embedded in a fluid-saturated porous medium. In our previous paper [1] we considered small g-jitter amplitudes and presented numerical and asymptotic solutions in terms of an expansion in powers of the small-amplitude parameter. Our objective here is to develop the basic understanding of the g-jitter effect begun in [1] by extending the analysis to g-jitter amplitudes which are comparable with gravity. As in [1] we confine our interest to those cases where Darcy's law is valid. Instead of a small-amplitude expansion, we reduce the governing equations to a system involving only two independent variables by means of a Fourier expansion in time. We find that strong g-jitter effects are confined mainly to the leading region, and these effects wane with distance downstream.

2. Governing equations and analysis

The nondimensional equations of motion for two dimensional convective boundary layer flow in a porous medium in the presence of g-jitter are given by (see [1])

$$\psi_{yy} = (1 + \epsilon \cos \omega t)\theta_y, \tag{1a}$$

$$\theta_t = \theta_{yy} + \psi_x \theta_y - \psi_y \theta_x. \tag{1b}$$

Here Darcy's law and the Boussinesq approximation are both assumed to be valid, and all the variables in (1a) and (1b) have been nondimensionalised as in [15]. Here, x is the streamwise coordinate along the heated vertical surface which is maintained at a nondimensional temperature $\theta = 1$, and y is the variable which is perpendicular to the surface. Far from the heated surface $\theta \to 0$ and the nondimensional streamfunction is taken to be zero on the heated surface $y = 0$. The quantities ω and ϵ are the frequency and amplitude of the g-jitter effect. The steady boundary layer flow which arises when $\epsilon = 0$ was first given by Cheng and Minkowycz [16] in terms of a similarity solution. They found that

$$\psi \sim x^{1/2} f(\eta), \quad \theta \sim g(\eta), \tag{2}$$

where the similarity variable, η, is defined as $\eta = y/x^{1/2}$. Given the present time-dependent forcing, we substitute

$$\psi \sim x^{1/2} f(\eta, t), \quad \theta \sim g(\eta, t) \tag{3}$$

into Eq. (1) and obtain

$$f'' = g'(1 + \epsilon \cos \omega t) \tag{4a}$$

and

$$g'' + \tfrac{1}{2} f g' = x(f' g_x - f_x g') + x g_t. \tag{4b}$$

Here primes denote derivatives with respect to η and the t and x subscripts represent derivatives with respect to those variables. The boundary conditions required to complete the specification of the mathematical problem are that

$$f = 0, \ g = 1 \ \text{ at } \eta = 0 \quad \text{and} \quad f', g \to 0 \ \text{ as } \eta \to \infty. \tag{5}$$

We note that Eq. (4a) may be integrated once with respect to η to reduce the system to third-order.

The solution of Eqs. (4) and (5) were found by first using the transformations:

$$\tau = \omega t, \quad \xi = \omega x, \tag{6}$$

which removes ω from the governing equations. Now f and g are expanded using the following Fourier series:

$$f = f_{0c}(\eta, \xi) + \sum_{n=1}^{N} [f_{nc}(\eta, \xi) \cos n\tau + f_{ns}(\eta, \xi) \sin n\tau], \tag{7a}$$

$$g = g_{0c}(\eta, \xi) + \sum_{n=1}^{N} [g_{nc}(\eta, \xi) \cos n\tau + g_{ns}(\eta, \xi) \sin n\tau]. \tag{7b}$$

After substitution of these series into the governing equations we obtain the following system of equations

$$f'_{0c} = g_{0c} + \tfrac{1}{2}\epsilon g_{1c}, \tag{8a}$$

$$f'_{1c} = g_{1c} + \epsilon\left[g_{0c} + \tfrac{1}{2} g_{2c}\right], \tag{8b}$$

$$f'_{1s} = g_{1s} + \tfrac{1}{2}\epsilon g_{2c}, \tag{8c}$$

$$f'_{nc} = g_{nc} + \tfrac{1}{2}\epsilon[g_{n-1,c} + g_{n+1,c}] \quad \text{for } n = 1, \ldots, N-1, \tag{8d}$$

$$f'_{ns} = g_{ns} + \tfrac{1}{2}\epsilon[g_{n-1,s} + g_{n+1,s}] \quad \text{for } n = 1, \ldots, N-1, \tag{8e}$$

$$f'_{Nc} = g_{Nc} + \tfrac{1}{2}\epsilon g_{N-1,c}, \tag{8f}$$

$$f'_{Ns} = g_{Ns} + \tfrac{1}{2}\epsilon g_{N-1,s}, \tag{8g}$$

$$g''_{0c} + \mathscr{L}^{0c}_{0c} + \frac{1}{2}\sum_{j=1}^{N}\left(\mathscr{L}^{jc}_{jc} + \mathscr{L}^{js}_{js}\right) = 0, \tag{9a}$$

$$g''_{1c} + \mathscr{L}^{0c}_{1c} + \mathscr{L}^{1c}_{0c} + \frac{1}{2}\sum_{j=1}^{N-1}\left[\mathscr{L}^{jc}_{j+1,c} + \mathscr{L}^{j+1,c}_{jc} + \mathscr{L}^{js}_{j+1,s} + \mathscr{L}^{j+1,s}_{js}\right] = \xi g_{1s}, \tag{9b}$$

$$g''_{1s} + \mathscr{L}^{0c}_{1s} + \mathscr{L}^{1s}_{0c} + \frac{1}{2}\sum_{j=1}^{N-1}\left[\mathscr{L}^{jc}_{j+1,s} - \mathscr{L}^{j+1,c}_{js} - \mathscr{L}^{js}_{j+1,c} + \mathscr{L}^{j+1,s}_{jc}\right] = -\xi g_{1c}, \tag{9c}$$

$$g''_{nc} + \mathscr{L}^{0c}_{nc} + \mathscr{L}^{nc}_{0c} + \frac{1}{2}\sum_{j=1}^{N-n}\left[\mathscr{L}^{j+n,c}_{jc} + \mathscr{L}^{jc}_{j+n,c} + \mathscr{L}^{j+n,s}_{js} + \mathscr{L}^{js}_{j+n,s}\right] + \frac{1}{2}\sum_{j=1}^{n-1}\left[\mathscr{L}^{n-j,c}_{jc} - \mathscr{L}^{n-j,s}_{js}\right] = n\xi g_{ns} \quad \text{for } n = 2,\ldots N-1, \tag{9d}$$

$$g''_{ns} + \mathscr{L}^{0c}_{ns} + \mathscr{L}^{ns}_{0c} + \frac{1}{2}\sum_{j=1}^{N-n}\left[\mathscr{L}^{jc}_{j+n,s} - \mathscr{L}^{j+n,c}_{js} - \mathscr{L}^{js}_{j+n,c} + \mathscr{L}^{j+n,s}_{jc}\right] + \frac{1}{2}\sum_{j=1}^{n-1}\left[\mathscr{L}^{n-j,s}_{jc} + \mathscr{L}^{n-j,c}_{js}\right] = -n\xi g_{nc} \quad \text{for } n = 2,\ldots N-1, \tag{9e}$$

$$g''_{Nc} + \mathscr{L}^{0c}_{Nc} + \mathscr{L}^{Nc}_{0c} + \frac{1}{2}\sum_{j=1}^{N-1}\left[\mathscr{L}^{jc}_{N-j,c} - \mathscr{L}^{js}_{N-j,s}\right] = N\xi g_{Ns}, \tag{9f}$$

$$g''_{Ns} + \mathscr{L}^{0c}_{Ns} + \mathscr{L}^{Ns}_{0c} + \frac{1}{2}\sum_{j=1}^{N-1}\left[\mathscr{L}^{jc}_{N-j,s} + \mathscr{L}^{js}_{N-j,c}\right] = -N\xi g_{Nc}. \tag{9g}$$

Here the operator $\mathscr{L}$ is defined according to

$$\mathscr{L}^{a}_{b} = \tfrac{1}{2} f_a g'_b - x(f'_a g_{b\xi} - f_{a\xi} g'_b), \tag{10}$$

where ξ-subscripts denote derivatives with respect to ξ.

Of interest to engineers is the mean rate of heat transfer, and therefore the sinusoidal components of the solution for g are not relevant for this purpose. Thus the time averaged rate of heat transfer may be obtained from the leading term in (7b), namely, $g'_{0c}(\eta = 0)$. If we define $Q(\xi)$ as a scaled global rate of heat transfer according to

$$Q(\xi) = \frac{\omega^{1/2}}{2\xi^{1/2}} \int_0^{\xi} \frac{\partial\theta}{\partial y}(x,y)\bigg|_{y=0} \mathrm{d}x \tag{11a}$$

then it may be shown that

$$Q(\xi) = \frac{1}{2\xi^{1/2}} \int_0^{\xi} \left[\frac{g'_{0c}(\eta,x)}{x^{1/2}}\right]_{\eta=0} \mathrm{d}x. \tag{11b}$$

When $\epsilon = 0$ we have $Q = -0.44376$ which agrees with that reported by Cheng and Minkowycz [16].

3. Numerical results

The whole system (8) and (9) comprises a set of parabolic partial differential equations which were solved using the Keller–box method [17]. Details of the method may be found in many recent publications by the present authors, and here we have used the semi-automatic procedure outlined in [18]. All the results quoted here were obtained using uniform grids in both the ξ and η directions; we took 200 intervals to cover $0 < x < 20$ and 100 intervals for $0 < \eta < 10$. This range of values of η is more than sufficient to contain the developing boundary layer. We found that very small steps in x were required to avoid pointwise oscillations in the streamwise direction, and, in order to obtain reasonable computation times, we modified the Keller box method to use a first order accurate backward difference discretisation in the x-direction. Although this is formally less accurate than is central differencing, we found that there were at least four figures of accuracy in our results. We also chose to use $N = 5$ as the truncation level for the Fourier series; again, this was sufficient to capture adequately the resolution of the flow near the leading edge where higher Fourier components are largest. Thus we solve a 33rd order system of partial differential equations. We also found that the backward differencing strategy allows computations to proceed for cases where $\epsilon > 1$, i.e. for cases where the perceived gravitational acceleration changes sign during each cycle; this is in contrast to the more usual centrally differenced method for which $\epsilon = 1$ was found to represent the maximum amplitude for which solutions may be obtained.

Firstly we needed to ensure that the complicated set of equations given in (8) and (9) have been encoded correctly, and this was done by comparing our numerical results with those of Rees and Pop [1] who considered asymptotically small amplitudes of g-jitter. While the equations solved in [1] display some similarity to those considered here, there are substantial differences between the two systems, and the subroutine which evaluates the finite difference approximation to Eqs. (8) and (9) was completely re-written in order that this check may be made. Likewise we modified the code used in [1] to use backward differences; the way in which that code is written allows such a modification to be made without changing those lines which define the equations to be solved. The results of this process are shown in Table 1 which compares the value of the $O(\epsilon)$ surface rate of heat transfer for the cosine term from [1] with the values of g'_{1c}/ϵ at both $\eta = 0$ and $\xi = 0$. A careful examination of the entries in Table 1 also shows that there is an $O(\epsilon^2)$ variation in $g'_{1c}/\epsilon|_{\eta=0}$ when ϵ is small; this is consistent with the fact that the next $\cos\tau$ term in [1] arises at $O(\epsilon^3)$. A more stringent test is the comparison of the evolution with ξ of the rates of heat transfer

Table 1
Comparison of the leading edge rate of heat transfer corresponding to the $\cos\tau$ term and the corresponding $O(\epsilon)$ term from [1] which is denoted by an asterisk

ϵ	$(g'_{1c}\|\eta=0)/\epsilon$
0.0*	−0.2214
0.1	−0.2216
0.2	−0.2222
0.3	−0.2232
0.4	−0.2247
0.5	−0.2267
0.6	−0.2293
0.7	−0.2327
0.8	−0.2372
0.9	−0.2429
1.0	−0.2506

corresponding to g'_{1c} and g'_{1s} with the corresponding $O(\epsilon)$ solutions from [1]. These are shown in Fig. 1 where the small-ϵ solution is compared with the solutions for $\epsilon = 0.2$, 0.4 and 1.0. Here we see clearly that the $\epsilon = 0.2$ curves are almost identical to the small-ϵ curve. In fact, the curve for $\epsilon = 0.1$ (not shown) is indistinguishable graphically from the small-ϵ curve.

Fig. 2 displays the behaviour of the local rate of heat transfer, $g'_{0c}|_{\eta=0}$, as a function of ξ for $\epsilon = 0.0$, 0.2, 0.4, 0.6, 0.8 and 1.0. This quantity is of interest since it corresponds to the mean value over time. For small values of ϵ we see that the deviation from the $\epsilon = 0$ curve is approximately quadratic, which gives good qualitative

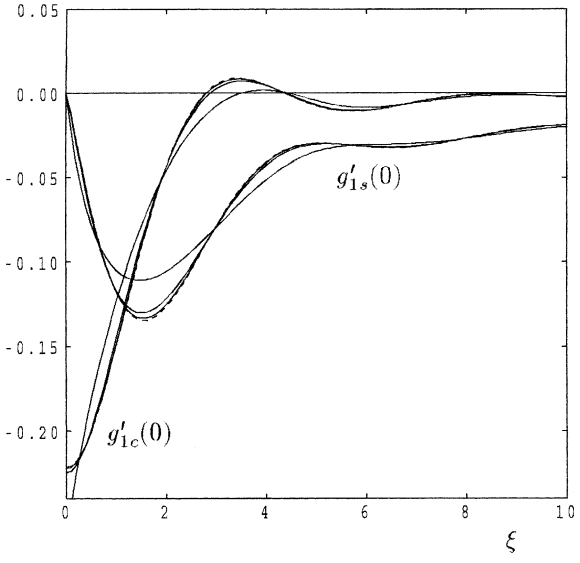

Fig. 1. The computed $O(\epsilon)$ rates of heat of transfer, $g'_{1c}(0)$ and $g'_{1s}(0)$, as functions of ξ from [1] (dashed curves), together with the corresponding curves for $\epsilon = 0.2$, 0.4 and 1.0. The curve corresponding to $\epsilon = 0.2$ is the closest continuous curve to the dashed curve.

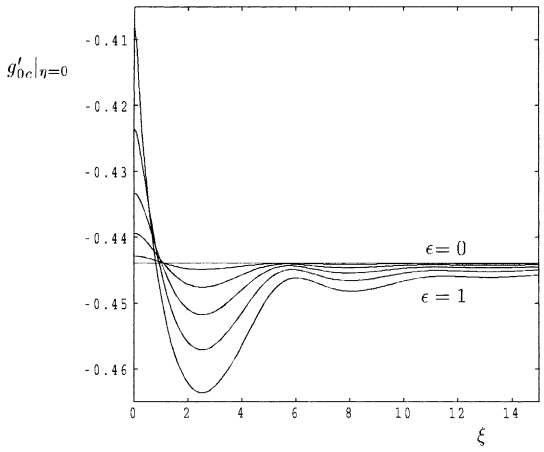

Fig. 2. The variation with ξ of the mean (i.e. time-averaged) local surface rate of heat transfer, $g'_{0c}|_{\eta=0}$, for $\epsilon = 0$, 0.2, 0.4, 0.6, 0.8 and 1.0.

agreement with the analysis of [1]. At larger values of the deviation becomes roughly linear. There is a distinctive decaying oscillation to an asymptotically decaying state which corresponds to the mean $O(\epsilon^2)$ solution given in Fig. 2 of [1]. The corresponding global rate of heat transfer is given in Fig. 3 for the same range of amplitudes. The main feature of these graphs is that the overall effect of g-jitter is to diminish the magnitude of the mean rate of heat transfer near the leading edge. It appears therefore that the decelerating phase of the g-jitter cycle reduces the mean rate of heat transfer by a greater amount than it is increased during the accelerating phase.

Figs. 4 and 5 show how the $\cos\tau$ and $\sin\tau$ components of the surface rate of heat transfer vary with ξ. In

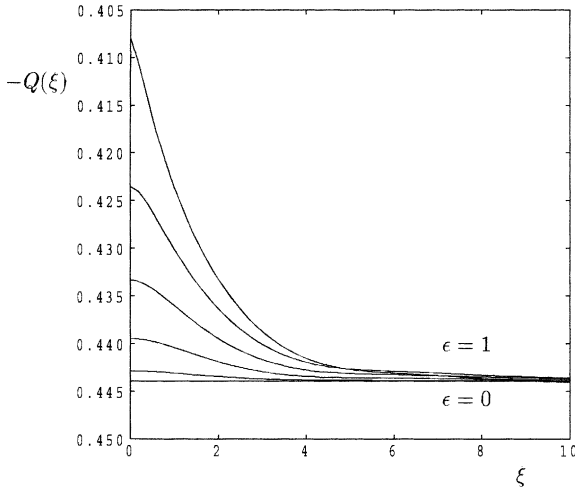

Fig. 3. The variation with ξ of the mean global surface rate of heat transfer, $Q(\xi)$, for $\epsilon = 0$, 0.2, 0.4, 0.6, 0.8 and 1.0.

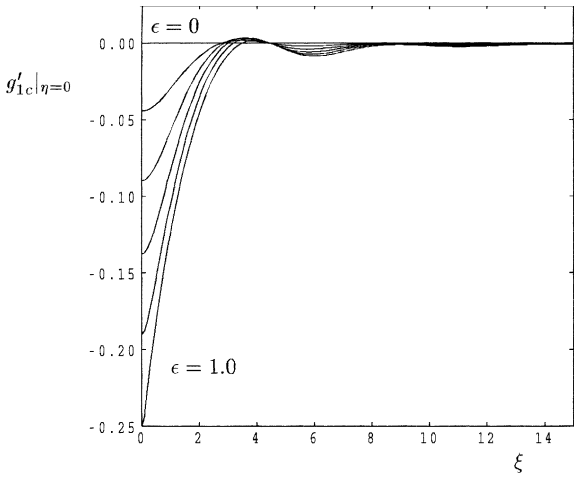

Fig. 4. The variation with ξ of the $\cos\tau$ (or in-phase) component of the local surface rate of heat transfer, $g'_{1c}|_{\eta=0}$, for $\epsilon = 0$, 0.2, 0.4, 0.6, 0.8 and 1.0.

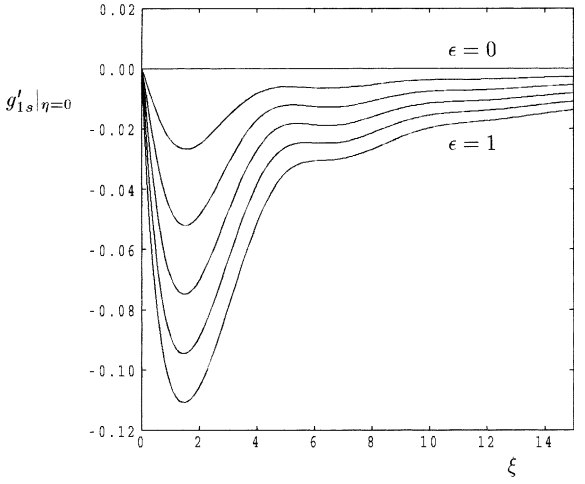

Fig. 5. The variation with ξ of the $\sin\tau$ (or out-of-phase) component of the local surface rate of heat transfer, $g'_{1s}|_{\eta=0}$, for $\epsilon = 0$, 0.2, 0.4, 0.6, 0.8 and 1.0.

both cases the primary effect of g-jitter is felt relatively close to the leading edge, but the in-phase ($\cos\tau$) component is much stronger than the out-of-phase ($\sin\tau$) component at the leading edge. A little further downstream, at $\xi = 2$, the out-of-phase component reaches its maximum strength, but at greater distances the out-of-phase component dominates and the response of the boundary-layer to the g-jitter forcing has a time lag of $\pi/2$ relative to the phase of the forcing. This is seen clearly in Fig. 6 where we display a contour plot of the time-varying local surface rate of heat transfer, $g'(\xi,\eta,\tau)|_{\eta=0}$ for $\epsilon = 0.2$. In this figure the horizontal axis corresponds to the leading edge, the maximum magnitude of the rate of heat transfer over time occurs

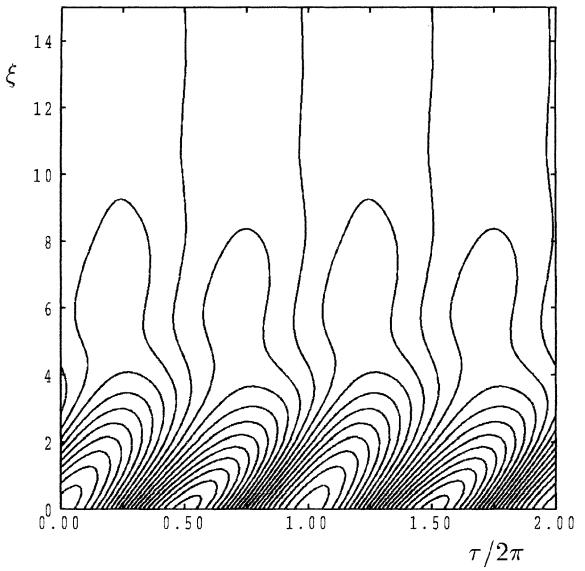

Fig. 6. Contours of the surface rate of heat transfer $g'(\xi,\eta,\tau)|_{\eta=0}$ for the case $\epsilon = 0.2$. If $b = 0.44376$, then the interval between contours is equal to $0.01b$. The contours reaching $\xi = 15$ correspond to $g'|_{\eta=0} = -b$ and the contour nearest to $\xi = \tau = 0$ corresponds to $-1.09b$.

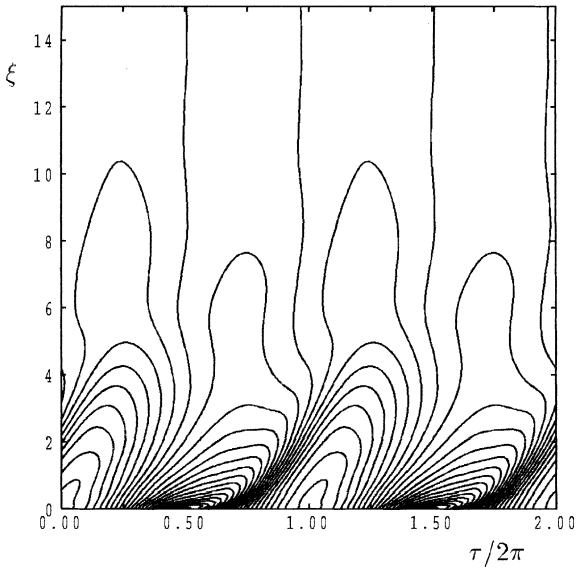

Fig. 7. Contours of the surface rate of heat transfer $g'(\xi,\eta,\tau)|_{\eta=0}$. The interval between contours is equal to $0.05b$; see the caption in Fig. 6. The contours reaching $\xi = 15$ correspond to $g'|_{\eta=0} = -b$ and the contour nearest to $\xi = \tau = 0$ corresponds to $-1.4b$.

at $\tau/2\pi = 0$, 1, 2, etc., and the minima occur at $\tau/2\pi = 0.5$, 1.5, 2.5, etc. The response of the boundary layer at larger distances has its maximum and minimum

magnitudes located at increasing values of τ relative to the leading edge, but the response also decays with ξ. The contours which 'survive' until $\xi = 15$ correspond to the constant value of $g'|_{\eta=0}$ which is obtained when there is no g-jitter effect (i.e. for $\epsilon = 0$). For the fairly small value of ϵ represented in Fig. 6 the time-dependent response is dominated by the $\cos\tau$ and $\sin\tau$ components. But at larger values of ϵ, such as is shown in Fig. 7 where $\epsilon = 1$, there is marked difference in the appearance of the contours between the accelerating and decelerating parts of the jitter cycle. This is because more Fourier modes become significant. Indeed, if we wished to compute the response to g-jitter with amplitudes greater than unity, it would be necessary to use a much larger number of Fourier modes. Once more, at the leading edge, the response achieves its maximum magnitude at times which are exactly in phase with the perceived gravitational acceleration, and there is an eventual $\pi/2$ phase shift at relatively large values of ξ.

4. Discussion

We have considered how vertical free convection in a porous medium is affected by large sinusoidal variations in the force of gravity about its mean value. The governing nonsimilar boundary layer equations were solved using a Fourier series expansion and the parabolic solver, the Keller-box method. Solutions have been presented in terms of the surface rate of heat transfer.

As in [1] it was found that the deviation from steady solutions corresponding to no g-jitter is most significant near the leading edge, and that the effect of g-jitter, at least in terms of the surface rate of heat transfer, decays with distance from the leading edge. When the g-jitter amplitude, ϵ, is small, the deviation from the mean $\epsilon = 0$ case is roughly sinusoidal. The peak rate of heat transfer, for instance, is in phase with the g-jitter forcing at the leading edge, but it varies monotonically to a $\pi/2$ phase lag with increasing distance. When ϵ takes values close to unity the response to g-jitter becomes strongly nonlinear and this effect is felt more during deceleration when the boundary layer thickens substantially and there is a very marked drop in the surface rate of heat transfer.

Acknowledgements

The authors wish to express their thanks to The Royal Society of London for partial financial support of the research undertaken in this paper.

References

[1] D.A.S. Rees, I. Pop, The effect of g-jitter on vertical free convection media boundary-layer flow in porous media, Int. Comm. Heat Mass Transfer 27 (2000) 415–424.
[2] D.A. Nield, A. Bejan, Convection in Porous Media, second ed., Springer, New York, 1999.
[3] D.B. Ingham, I. Pop (Eds.), Transport Phenomena in Porous Media, Pergamon, Oxford, 1998.
[4] K. Vafai (Ed.), Handbook of Porous Media, Begell House, New York, 2000.
[5] J.I.D. Alexander, Low gravity experiment sensitivity to residual acceleration: A review, Microgravity Sci. Technol. III 2 (1990) 52–68.
[6] E.S. Nelson, An examination of anticipated g-jitter on space station and its effects on materials processing, NASA Tech. Mem. 103775, 1991.
[7] N. Amin, The effect of g-jitter on heat transfer, Proc. R. Soc. Lond. A 419 (1988) 151–172.
[8] S. Biringen, G. Danabasoglu, Computation of convective flow with gravity modulation in rectangular cavities, J. Thermophys. Heat Transfer 4 (1990) 357–365.
[9] S. Biringen, L.J. Peltier, Computational study of 3-D Benard convection with gravitational modulation, Phys. Fluids A 2 (1990) 279–283.
[10] J.I.D. Alexander, S. Amiroudine, J. Ouzzani, F. Rosenberger, Analysis of the low gravity tolerance of Bridgman-Stockbarger crystal growth, J. Cryst. Growth 113 (1991) 21–38.
[11] A. Farooq, G.M. Homsy, Streaming flows due to g-jitter-induced natural convection, J. Fluid Mech. 271 (1994) 351–378.
[12] A. Farooq, G.M. Homsy, Linear and nonlinear dynamics of a differentially heated slot under gravity modulation, J. Fluid Mech. 313 (1996) 1–38.
[13] B.Q. Li, g-jitter induced free convection in a transverse magnetic field, Int. J. Heat Mass Transfer 39 (1996) 2853–2860.
[14] B. Pan, B.Q. Li, Effect of magnetic fields on oscillating mixed convection, Int. J. Heat Mass Transfer 41 (1998) 2705–2710.
[15] D.S. Riley, D.A.S. Rees, Non-Darcy natural convection from arbitrarily inclined heated surfaces in saturated porous media, Q. J. Mech. Appl. Math. 38 (1985) 277–295.
[16] P. Cheng, W.J. Minkowycz, Free convection about a vertical flat plate embedded in a porous medium with application to heat transfer from a dyke, J. Geophys. Res. 82 (1977) 2040–2044.
[17] H.B. Keller, T. Cebeci, Accurate numerical methods for boundary layer flows 1. Two dimensional flows, in: Proceedings of International Conference Numerical Methods in Fluid Dynamics, Lecture Notes in Physics, Springer, New York, 1971.
[18] D.A.S. Rees, Three-dimensional free convection boundary layers in porous media induced by a heated surface with spanwise temperature variations, Trans. ASME J. Heat Transfer 119 (1997) 792–798.